

Article

Piezoelectric Response and Cycling Fatigue Resistance of Low-Temperature Sintered PZT-Based Ceramics

Zirui Lin ¹, Zhe Zhu ¹, Zhonghua Yao ^{1,2,*} , Hao Zhang ¹, Hua Hao ^{1,2}, Minghe Cao ¹ and Hanxing Liu ^{1,2}¹ School of Material Science and Engineering, Wuhan University of Technology, Wuhan 430070, China² Sanya Science and Education Innovation Park of Wuhan University of Technology, Wuhan 430070, China

* Correspondence: yaozhhua@whut.edu.cn

Abstract: The preparation of low-cost multilayer piezoelectric devices requires using cheap internal electrodes between the dielectric layers. A general strategy is to reduce the sintering temperature T_s of the ceramic layer by sintering aids which can form a liquid phase. Here, 0.2 wt% Li_2CO_3 was added as a sintering aid to tailor the sinterability and piezoelectricity of the commercial PZT ceramics. As verified from experiments, the piezoelectric ceramics could be densified at a sintering temperature above 940 °C, suitable for co-firing with the cheap internal electrode. The optimized sintering temperature of 980 °C can be confirmed for the 0.2 wt% Li_2CO_3 -modified PZT ceramics due to its high piezoelectric coefficient $d_{33} \sim 701$ pC/N, planar coupling factor $k_p \sim 66.7\%$, and a low mechanical quality factor $Q_m \sim 71$ with a transition temperature of $T_c \sim 226$ °C, presenting the characteristics of typical soft piezoelectric ceramics. Moreover, both the potential piezoelectric strain $\sim 0.13\%$ under 20 kV/cm and the good cycling fatigue characteristic ($>10^4$ cycles) of the studied piezo compositions indicates strong competitiveness in the field of multilayer piezoelectric devices.

Keywords: ceramics; sintering aids; piezoelectric ceramics; multilayer

Citation: Lin, Z.; Zhu, Z.; Yao, Z.; Zhang, H.; Hao, H.; Cao, M.; Liu, H. Piezoelectric Response and Cycling Fatigue Resistance of Low-Temperature Sintered PZT-Based Ceramics. *Materials* **2023**, *16*, 1679. <https://doi.org/10.3390/ma16041679>

Academic Editors: Yuhang Ren and Jun Ouyang

Received: 9 January 2023

Revised: 15 February 2023

Accepted: 16 February 2023

Published: 17 February 2023



Copyright: © 2023 by the authors. Licensee MDPI, Basel, Switzerland. This article is an open access article distributed under the terms and conditions of the Creative Commons Attribution (CC BY) license (<https://creativecommons.org/licenses/by/4.0/>).

1. Introduction

Piezoceramics come from the general design of ferroelectrics due to the piezoelectric effect via electric-field-driven polarization treatment of polycrystals. These piezoelectric effects can generate an electro-response or micro-displacement response, which can be used for electronic components and devices for displacement and electrical-signal sensitivity [1–3]. Compared to electromagnetic actuators, piezoelectric ceramics mainly feature compact size, low driving voltage, quick response, high efficiency, accurate position, etc. [4–7].

Chemical doping dominates the structural design of piezoelectric materials to form donor-type (soft) or acceptor-type (hard) characteristics. Doping high-valence ions (e.g., La^{3+} , Nd^{3+} , Sm^{3+} , Nb^{5+} and Ta^{5+}) always cause lead vacancies, which is beneficial to domain rotation during electric field polarization, and further improve dielectric, electromechanical, and piezoelectric properties, similar to softening ceramics [8–11]. Soft piezoelectric ceramics are characterized by high direct piezoelectric constant d_{33} , strain rate S , significant remnant polarization P_r , and low coercive field E_c . Typical soft Pb-based compositions by La doping, $\text{Pb}_{1-x}\text{La}_x(\text{Zr}_y\text{Ti}_{1-y})_{1-x/4}\text{O}_3$ (abbreviated as PLZT) ceramics have been extensively studied due to their high electromechanical and electro-optical properties. La/Zr/Ti ratio can make the PLZT ceramics own various phase structures such as ferroelectric, relaxor ferroelectric, antiferroelectric, and paraelectric phases for diverse applications. Wu et al. reported $\text{Pb}_{0.91}\text{La}_{0.06}(\text{Zr}_{0.58}\text{Ti}_{0.42})_{0.975}\text{Nb}_{0.02}\text{O}_3$ prepared via the ceramic injection molding (CIM) technique with ultra-high d_{33} (731 pC/N) [12]. Kumar et al. reported a high effective piezoelectric constant $d_{33}^* \sim 632$ pm/V and a high unipolar strain rate $S \sim 0.25\%$ in $\text{Pb}_{0.92}\text{La}_{0.08}(\text{Zr}_{0.60}\text{Ti}_{0.40})\text{O}_3$, accompanied by a high $P_r \sim 33$ $\mu\text{C}/\text{cm}^2$ and a low $E_c \sim 10$ kV [13]. As reported, Nb doping can compensate for

the vacancy at the B site for ABO₃-type perovskites caused by La doping. Nb-doping also has been proven to contribute to the improvement of piezoelectric responses and fatigue behavior, then the decrease in the coercive field [14,15]. In addition, Nb oxide is helpful to densify the Pb(Zr_{1-x}Ti_x)O₃ (abbreviated as PZT)-based piezoceramics and decrease the sintering temperature slightly [14].

A multilayered design can be instrumental in the increase in micrometric displacement and the reduction in the driving field of PZT-based piezoelectric devices [16]. Multilayer ceramics are designed to co-sinter the inner electrodes and tape-cast ceramic sheet layers together. Developing the multilayered design is essential to lower the cost of products via co-sintering ceramic layers with cheap electrode paste, such as pure Ag or high Ag/low Pd paste instead of expensive platinum (Pt)/palladium (Pd) electrode paste. However, the low-temperature stability of cheap metal electrode paste limits the co-sintering of traditional PZT-based systems due to high sintering temperatures above 1200 °C [17,18]. There are various strategies to lower the sintering temperature of PZT-based piezoceramics, such as nanosized powder sintering [19], liquid phase assisted sintering [20], cold sintering process [21], high-energy ball milling [22], etc. Among these, the most straightforward and economical method is to form a liquid phase by sintering aid. Metal oxides/carbonates, such as B₂O₃, CuO, Bi₂O₃, ZnO, and Li₂CO₃, are the most used sintering additives. Moreover, the complex sintering aids can make low-temperature sintering effective [23]. Zhang et al. confirmed that the combined use of LiBiO₂ and CuO has an excellent enhancement effect on d_{33}^* and optimal sinterability compared to pure LiBiO₂ [24]. Choi et al. investigated that the mixed 4PbO-B₂O₃ liquid frits could optimize the sintering temperature of 0.4Pb(Zn_{1/3}Nb_{2/3})O₃-0.6Pb(Zr_{0.47}Ti_{0.53})O₃ piezoceramics, providing a liquid phase at below 800 °C [25].

The mechanism of sintering aids is that it can form a liquid transitional phase at a relatively low temperature, which can facilitate the dissolution and migration of substances, accelerate grain growth, and finally be absorbed into the ceramic to form a solid solution in the lattice and impurity at the grain boundary. Donnelly et al. reported that Li₂CO₃ reacted with excess PbO to form an intermediate liquid phase, the Li₂PbO₃ phase, which subsequently melted at 836 °C, resulting in the promotion of particle rearrangement [26]. Siddiqui et al. studied the effect of Li₂CO₃ on Pb_{0.93}La_{0.02}Sr_{0.05}(Zr_{0.52}Ti_{0.48})O₃ (abbreviated as PLSZT) ceramics sintered at 850 °C. They found that the relative permittivity $\epsilon_r \sim 1270$ and the planar electromechanical couple factor $k_p \sim 46\%$ were enhanced compared to those without Li₂CO₃ sintered at 1150 °C ($\epsilon_r \sim 1145$, $k_p \sim 33\%$) [27]. However, d_{33} decreased from 315 pC/N for pure PLSZT to 259 pC/N for the modified one. Kim et al. reported that CuO-doped 0.69Pb(Zr_{0.47}Ti_{0.53})O₃-0.31[Pb(Zn_{0.4}Ni_{0.6})_{1/3}Nb_{2/3}]O₃ ceramics exhibited a higher strain of 0.165% than that 0.145% for undoped ones [28]. Zhang et al. revealed that Li⁺ could segregate at the grain boundaries and suppress grain growth of 15Pb(Sc_{1/2}Nb_{1/2})O₃-52Pb(Mg_{1/3}Nb_{2/3})O₃-33PbTiO₃ (abbreviated as PSN-PMN-PT) piezoceramics when excessive Li₂CO₃ was employed when sintered at 850 °C [29]. Both d_{33} and k_p increased from 465 pC/N and 60% for pure PSN-PMN-PT ceramics to 520 pC/N and 62% for 0.5 wt% Li₂CO₃-modified one, respectively. Some other examples of low-temperature piezoceramics are listed in Table 1. It has been reported that Li₂CO₃ is a typical sintering aid usually used in PZT-based ceramics. The effect of the content of sintering aids on lead-based piezoelectric ceramics has been experimentally and theoretically studied. Commonly, the addition of sintering aids can always decrease the sintering temperature at the expense of reducing piezoelectricity. In this work, an appropriate amount of 0.2 wt% Li₂CO₃ was chosen as the sintering aid of commercial soft PZT-based piezoceramics to develop the low-temperature cofired piezoelectric ceramic system. The modified ceramics can be cofired with cheap metal electrodes while retaining excellent piezoelectric response.

Table 1. Comparison of piezoelectric properties of PZT-based ceramics with sintering aids (T_s : sintering temperature; T_c : Curie temperature).

Sintering Aid	Ceramic Composition	T_s (°C)	T_c (°C)	d_{33} (pC/N)
Li ₂ CO ₃ (0.07 wt.%) + Fe ₂ O ₃ (0.25 wt.%) [30]	PZT-PZN-PMnN	1000		455
Li ₂ CO ₃ (0.2 wt.%) [31]	PNN-PZT	950	113	692
Li ₂ CO ₃ (0.3 wt.%) + Sm ₂ O ₃ (0.3 wt.%) [32]	0.3PZN-0.7PZT	900	394	483
Li ₂ CO ₃ (0.2 wt.%) + CaCO ₃ (0.3 wt.%) [33]	PNN-PMW-PZT	900	296	599
Li ₂ CO ₃ (0.2 wt.%) + CaCO ₃ (0.25 wt.%) + Ta ₂ O ₅ (0.7 wt.%) [34]	PNN-PMW-PZT	940	640	303
Yb ₂ O ₃ (0.1 mol%) [35]	PNN-PMW-PZT	900	179	623
Sm ₂ O ₃ (0.3 wt.%) + LiF (0.01%) [17]	PZN-PZT	950	289	403
Ba(Cu _{1/2} W _{1/2})O ₃ (0.1 wt.%) [36]	PNN-PMW-PSN-PZT	900	161	551

2. Materials and Methods

Commercial soft PZT-based (PZT-5H) piezoelectric powders (Xi'an Konghong New Material Technology Co., Ltd., Xi'an, China) were selected as the base materials, and the Li₂CO₃ (99% purity, Shanghai Aladdin Reagent Co., Ltd., Shanghai, China) was selected as the sintering aid. The base materials were designed to form the 0.2 wt% Li₂CO₃-modified compositions for fabricating low-temperature cofired ceramic devices. The mixed powders were milled with ethanol for one day. The calcination process was conducted at 850 °C for 2 h. The resultant powders were granulated with a 2.0 wt.% polyvinyl alcohol (PVA) aqueous solution. Pressing was carried out to form the disc samples 12 mm in diameter under 180 MPa. The binders were fired at 600 °C for 2 h, and then the ceramics were sintered from 900 °C to 1100 °C for 2 h.

The ceramics were ground and polished up to a thickness of 0.5 mm on sandpaper. Density measurement was conducted using the Archimedes method. Silver pastes with conducting compositions of 80% Ag and 3% Pd were coated and fired for 10 min at 580 °C on both sides of the samples. The poling of the samples was conducted in silicon oil at 120 °C for 30 min under 25 kV/cm. The ceramics were aged for one day before piezoelectric measurements. The crystal structure was determined by X-ray diffraction (XRD) with $CuK\alpha = 1.54\text{\AA}$. The microstructures were observed through a scanning electron microscope (SEM, JSM-6700F). The piezoelectric d_{33} was measured by a ZJ-3A quasi-static piezoelectric meter 1 pC/N, and 0.2 N. Dielectric property-temperature spectra were characterized by an E4980A LCR meter connected with the temperature control system (Partulab, DMS-1000) in the temperature range from RT to 500 °C at a heating rate of 2 °C/min. The S - E relations can be evaluated by a ferroelectric workstation (aixACCT, TF analyzer 2000) under 20 kV/cm electric field strength. The polarization-field (P - E) hysteresis loops were determined by the ferroelectric analyzer (PolyK, PK-CPE1701). The impedance $|Z|$ and phase angle θ were collected by the impedance analyzer (Agilent, HP4294A, Santa Clara, CA, USA). The k_p value was calculated according to Equation (1) [37]:

$$k_p = \frac{1}{\sqrt{0.395 \frac{f_r}{f_a - f_r} + 0.574}} \quad (1)$$

where f_r and f_a represent resonance and antiresonance frequencies, respectively, the mechanical quality factor Q_m was calculated by Equation (2):

$$Q_m = \frac{f_a^2}{2 \pi f_r R (c_0 + c_1) (f_a^2 - f_r^2)} \quad (2)$$

where R , c_1 , and c_0 are the minimum impedance at resonance, the capacitance of the ceramics at resonance, and the capacitance in an electrostatic field, respectively [37].

3. Results and Discussion

3.1. XRD Patterns

Figure 1 presents the phase structure of the sintered 0.2 wt% Li_2CO_3 -modified bulk ceramics. All of the specimens show the pure perovskite single phase without any impurity composition under the limit of X-ray detection. The broadening of the (200) peak is observed in the samples sintered at 900~1000 °C at the $2\theta = 44\text{--}46^\circ$ region, which is evidence of the coexistence of the tetragonal and rhombohedral phases. In other words, near the morphotropic phase boundary (MPB). It is generally believed that piezoelectric ceramics have the optimum piezoelectric properties near the MPB. When the sintering temperature increases, a distinct splitting of the $(002)_T$ and $(200)_T$ peaks can be observed, which implies that the coexistence of the rhombohedral-tetragonal phase near MPB tends to transform into the tetragonal-rich phase. As reported, this transformation can be attributed to the stress relaxation caused by the grain growth of piezoelectric ceramics [38,39]. The ferroelectric ceramics will form an inner stress conducive to the stability of the rhombohedral phase, as reported. However, with the increase of the grain size, the internal stress is challenging to continue to concentrate and finally turns into cracks, releasing this stress and resulting in the rise of tetragonal phases [40].

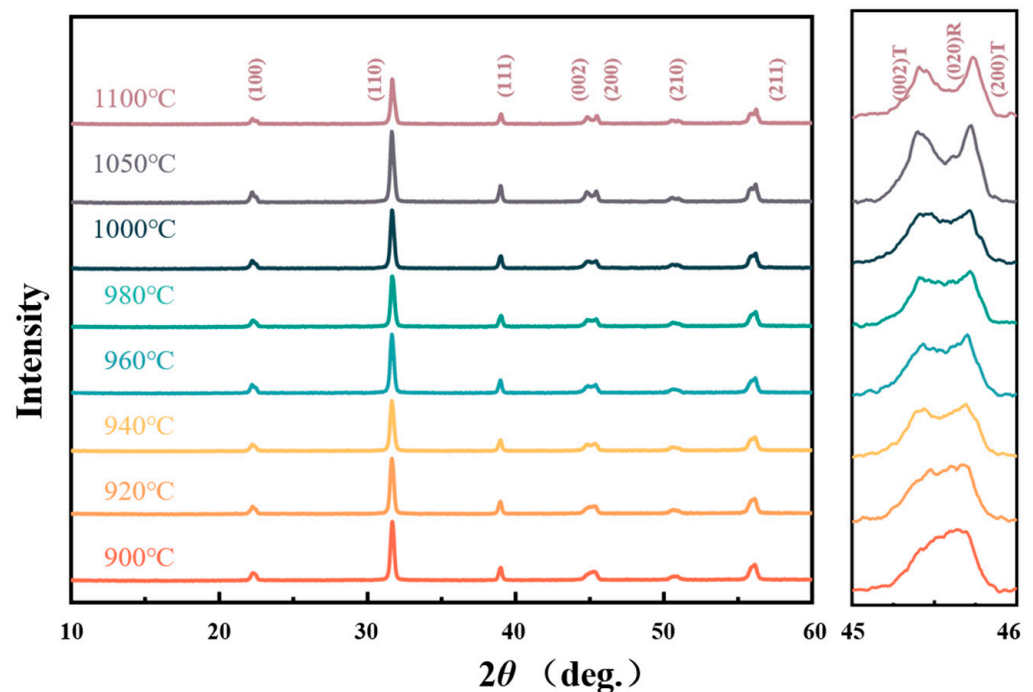


Figure 1. XRD patterns for the 0.2 wt% Li_2CO_3 -modified bulk ceramics.

3.2. SEM Images

Figure 2 shows the fractured cross-sectional SEM images and grain size distribution diagrams of the specimens at different sintering temperatures. Grain grows gradually, consistent with the sintering temperature. The average grain size of ceramic increases from 1.86 μm at 900 °C to 3.45 μm at 1100 °C. It can be observed that grain growth remains constant above 980 °C, with an average grain size of around 3.30 μm , similar to the previous report [31].

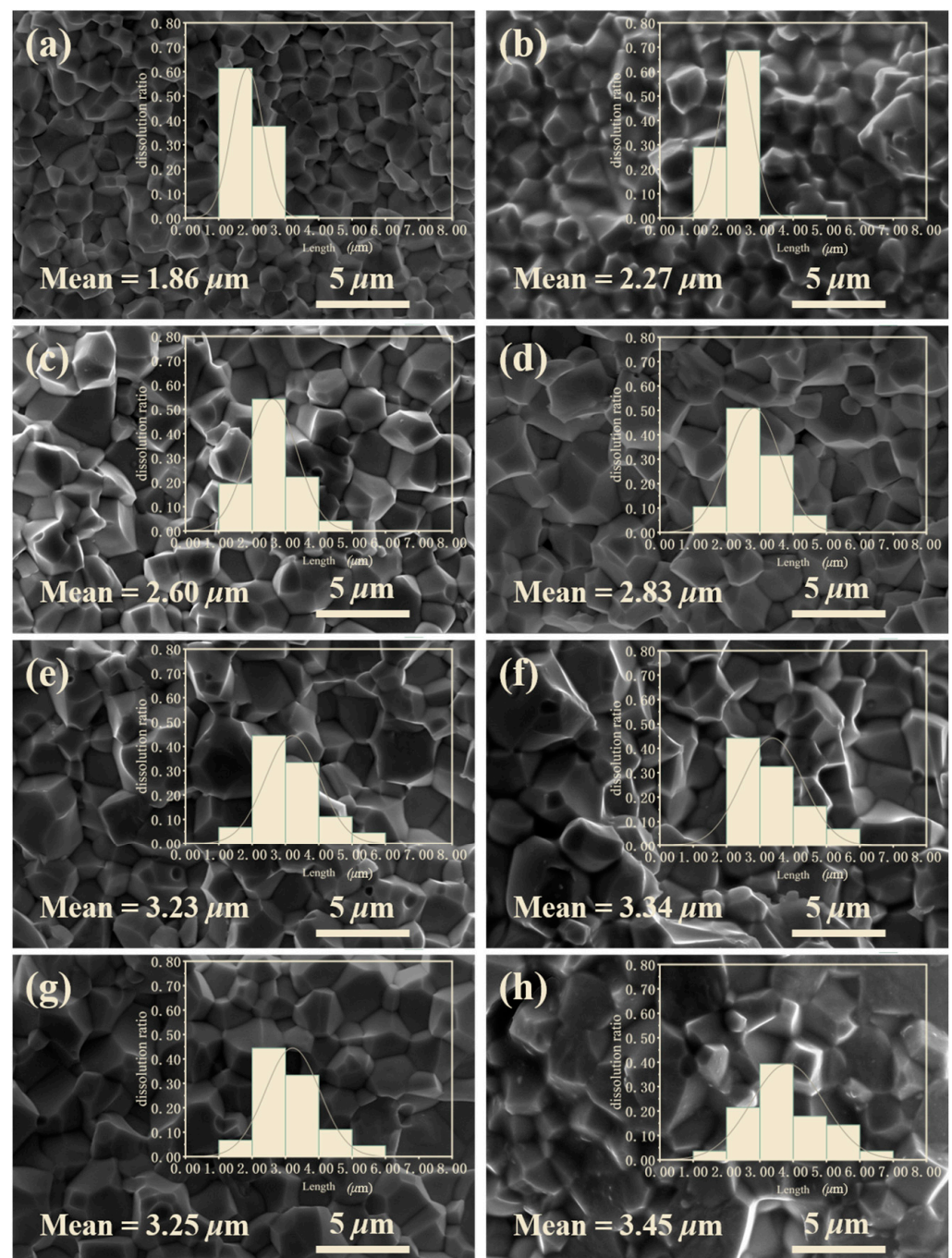


Figure 2. SEM images and grain size distribution for the 0.2 wt% Li_2CO_3 -modified ceramics sintered at various temperatures: (a) 900 °C; (b) 920 °C; (c) 940 °C; (d) 960 °C; (e) 980 °C; (f) 1000 °C; (g) 1050 °C; (h) 1100 °C.

Figure 3 depicts dielectric property-temperature spectra of the 0.2 wt% Li_2CO_3 -modified ceramics with various frequencies (100 Hz, 1 kHz, 10 kHz, and 100 kHz). With the increase in testing frequency, no shift or broadening of the dielectric peak was observed. Dielectric maximum peaks show sharp phase transitions indicative of a typical ferroelectric characteristic without any relaxor behavior. It can be concluded that the Curie temperature of the 0.2 wt% Li_2CO_3 -modified ceramics is around 226 °C. It can be deduced that piezoelectric devices based on these compositions can be used in temperatures above 110 °C. For that, the poled piezoelectric ceramics often begin to become unstable at a temperature somewhat above half the Curie temperature.

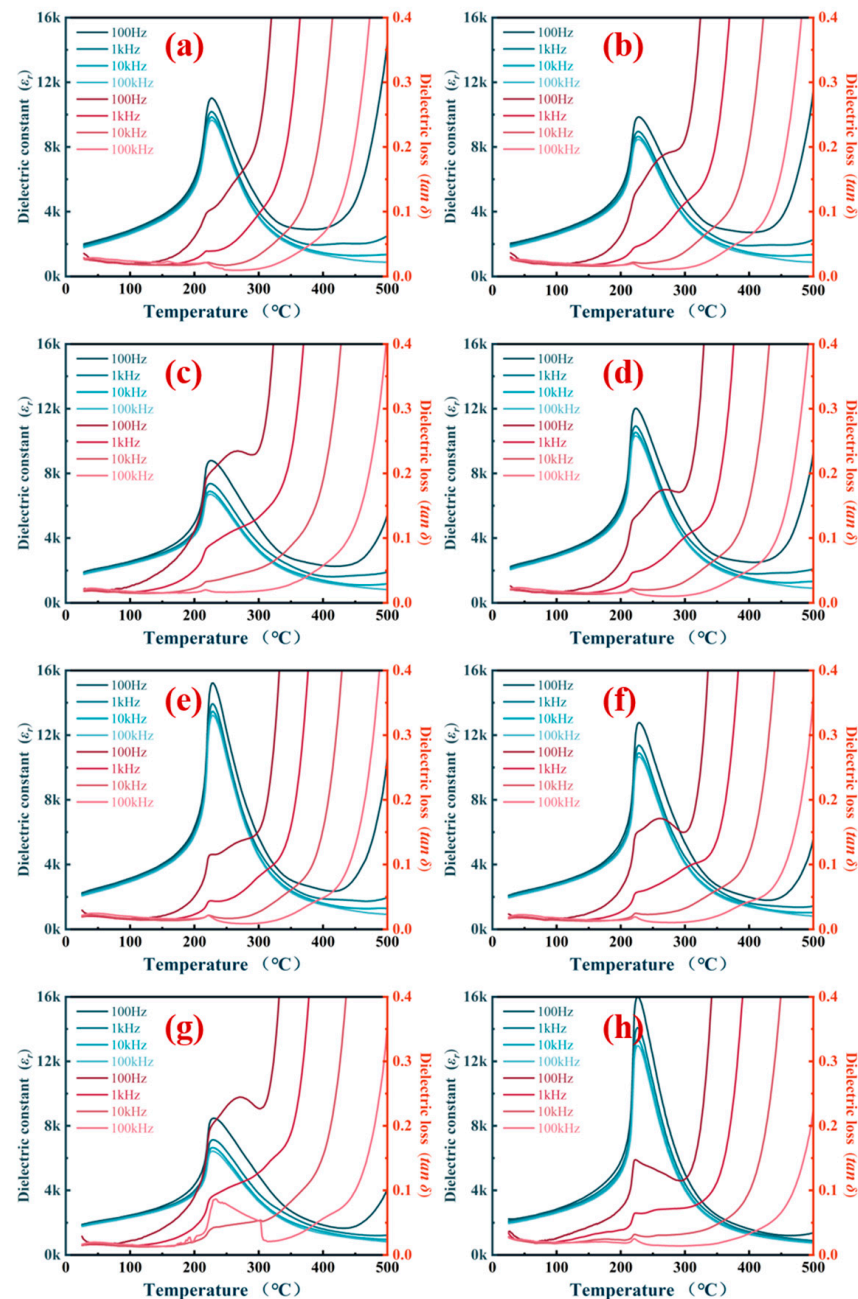


Figure 3. Dielectric property-temperature spectra of the 0.2 wt% Li_2CO_3 -modified ceramics sintered at different temperatures: (a) 900 °C; (b) 920 °C; (c) 940 °C; (d) 960 °C; (e) 980 °C; (f) 1000 °C; (g) 1050 °C; (h) 1100 °C.

The physical parameters of the studied ceramic samples, including k_p , Q_m , d_{33} , d_{33}^* , E_c , and P_r , are summarized in Table 2. The piezoceramics sintered at 980 °C have the optimal piezoelectric characteristics with a d_{33} of 701 pC/N and a k_p of 66.7%. Q_m values of all the samples remain constant at about 70, independent of sintering temperatures. Lead vacancies which are widely thought will result in low Q_m , making the ceramics “soft”. Lead vacancies are propitious to domain switching. Thus, soft piezoelectric ceramics feature quick response speed, high piezoelectric constant, and low mechanical quality factor value. As reported, it is hard to ensure that the ceramics sintered at low temperatures have a high Q_m [41]. At low sintering temperatures, the effect of temperature on lead/oxygen vacancies is far less than that of doping [42]. This should be responsible for the temperature independence for Q_m . The impedance plots are shown in Figure 4.

Table 2. The specific values of electrical parameters of the 0.2 wt% Li_2CO_3 -modified PZT-based ceramics.

$T_{\text{sintering}}$ ($^{\circ}\text{C}$)	T_c ($^{\circ}\text{C}$)	d_{33} pC/N	d_{33}^* pm/V	E_c kV/cm	P_r $\mu\text{C}/\text{cm}^2$	k_p (%)	Q_m
900	226	618	701	11.98	29.16	63.4	75
920	228	665	640	14.54	30.37	64.6	76
940	226	682	652	10.86	27.66	65.4	73
960	224	683	624	11.53	27.99	66.2	69
980	229	701	651	10.18	32.60	66.7	71
1000	229	661	648	11.28	27.68	66.3	70
1050	231	597	716	12.26	30.29	60.2	82
1100	226	591	721	10.03	30.12	58.1	78

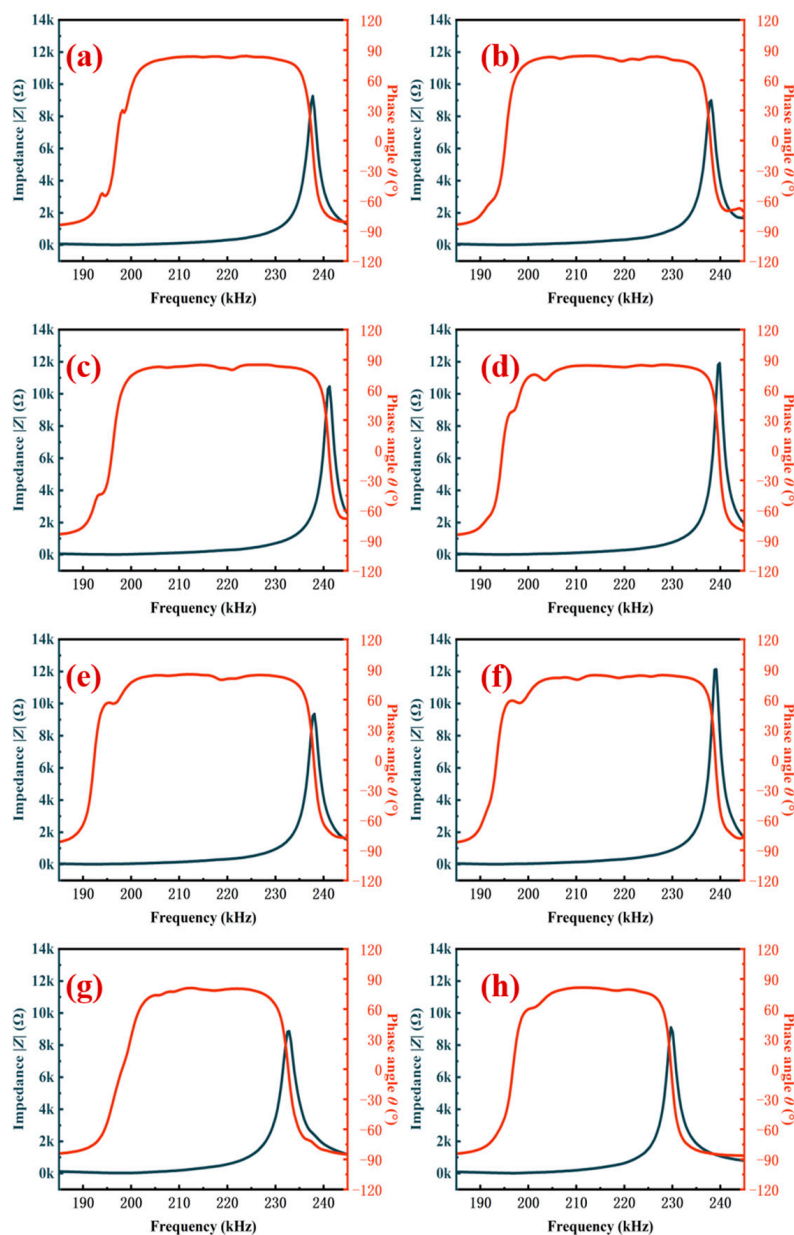


Figure 4. Impedance plots of the 0.2 wt% Li_2CO_3 -modified ceramics: (a) 900 $^{\circ}\text{C}$ sintered; (b) 920 $^{\circ}\text{C}$ sintered; (c) 940 $^{\circ}\text{C}$ sintered; (d) 960 $^{\circ}\text{C}$ sintered; (e) 980 $^{\circ}\text{C}$ sintered; (f) 1000 $^{\circ}\text{C}$ sintered; (g) 1050 $^{\circ}\text{C}$ sintered; (h) 1100 $^{\circ}\text{C}$ sintered.

Figure 5 illustrates the ferroelectric properties of the 0.2 wt% Li_2CO_3 -modified ceramics. To achieve polarization saturation, the specimens were tested under 40 kV/cm, which is about four times E_c . The maximum remnant polarization P_r ($32.60 \mu\text{C}/\text{cm}^2$) can be obtained for the ceramics sintered at 980 °C. The remnant polarization has almost the same trend as the d_{33} due to the relationship of $\epsilon_r P_r$.

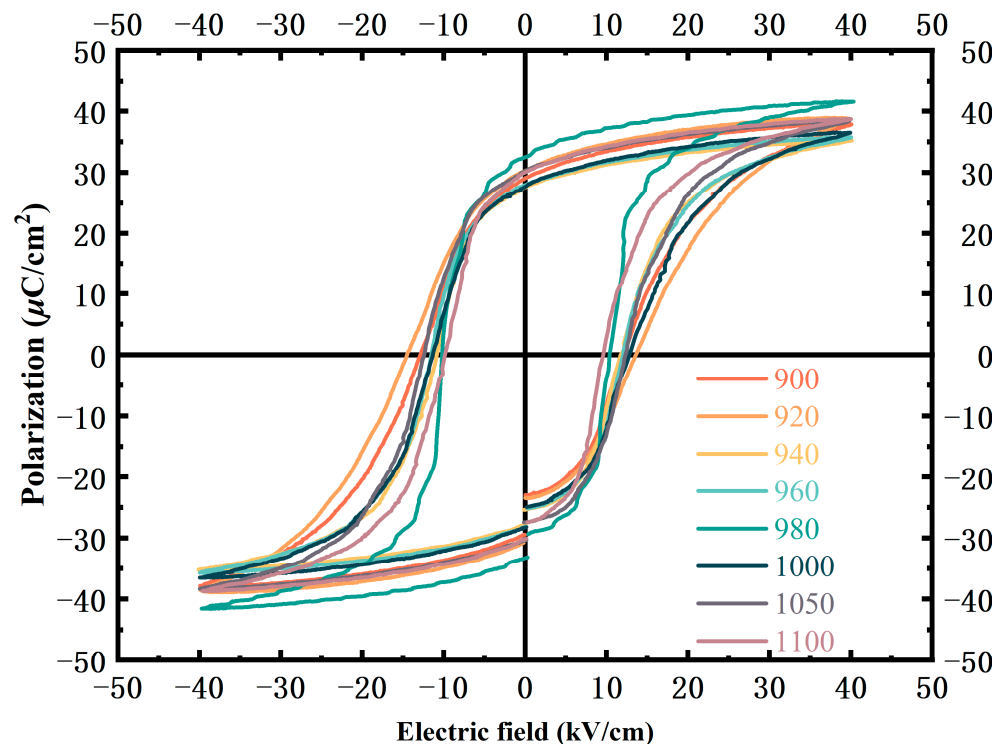


Figure 5. Ferroelectric hysteresis loop under 40 kV/cm.

As mentioned above, the piezoelectricity of the 0.2 wt% Li_2CO_3 -modified ceramics exhibits slight variation with the increase in sintering temperature. Ultrahigh piezoelectric properties can be obtained under a low sintering temperature below 1000 °C, facilitating the use of cheap metal in the cofired ceramic devices.

Figure 6a depicts the unipolar strain curves (S - E) of the 0.2 wt% Li_2CO_3 -modified ceramics under 20 kV/cm. The strain of the ceramics remains almost constant on the variation of sintering temperature in the range of 0.12–0.14%. The normalized strain large-signal longitudinal piezoelectric constant d_{33}^* can be calculated by Equation (3) and listed in Table 2.

$$d_{33}^* = \frac{S_{\max}}{E_{\max}} \quad (3)$$

Regardless of the difference in grain size, piezoelectric strain remains constant, indicative of the maximization of reversible 90° domain switching.

However, piezoelectric ceramics are very brittle and susceptible to fracture during the electric drive. The electric field applied to the ceramic commonly causes the volume expansion/shrinkage of the unit cell of the ceramics. The variation of lattice volume usually causes internal stress, easily leading to the crack of piezoceramics. Cyclic testing of unpoled piezoelectric ceramics effectively verifies the fatigue behavior of piezoelectric devices [43]. Here, a working electric field of 25 kV/cm was selected to determine the cyclic fatigue properties by P - E loops of piezoelectric ceramics in Figure 6b. The ceramic samples were tested by 10^4 times at 1 Hz with a triangle input signal. It can be observed that piezoelectric ceramics sintered at low temperatures become easy to dielectric breakdown, while the piezoelectric ceramics sintered above 960 °C can withstand 10^4 cycles of electric excitation. It suggests that a high sintering temperature for ceramics contributes to the enhancement

of fracture strength, possibly due to the improved bulk density or less porosity. It can be confirmed that the optimal T_s is near 960 °C, matching the sinterability of silver paste.

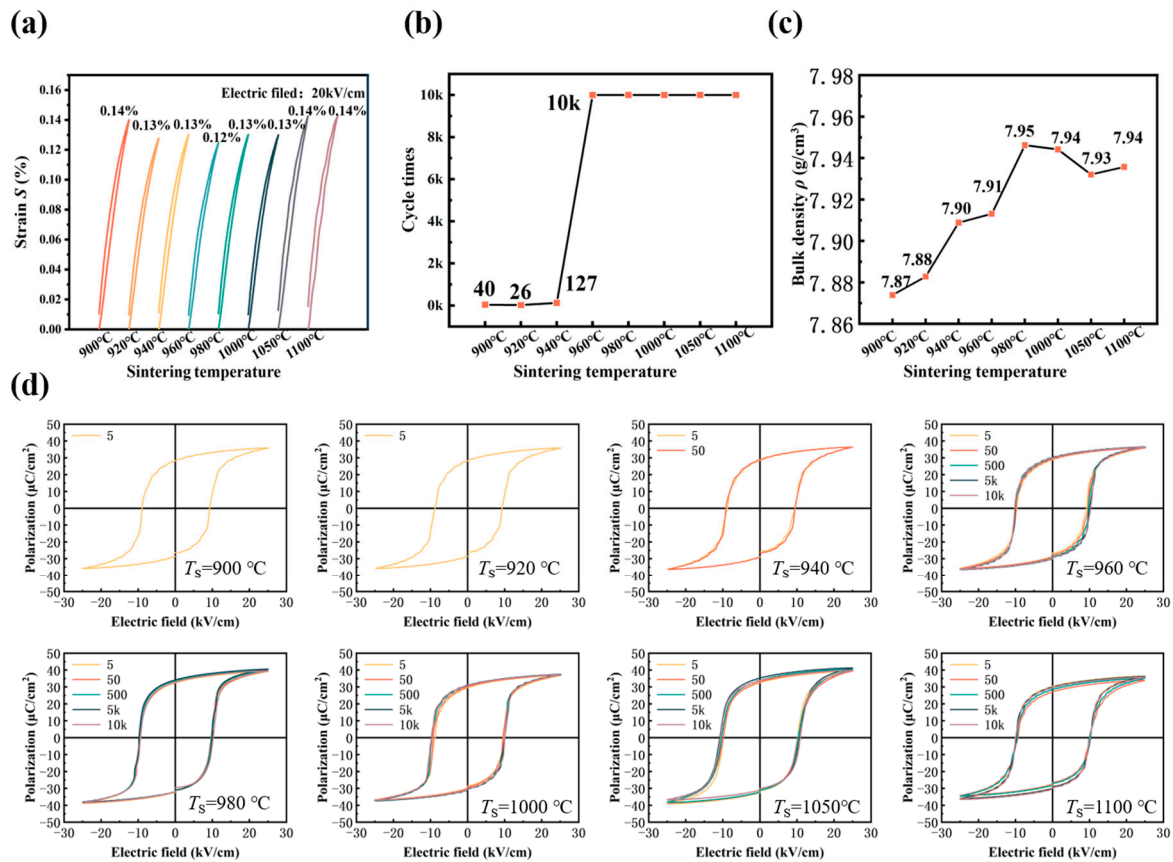


Figure 6. (a) Unipolar strain (S - E) curves of the 0.2 wt% Li_2CO_3 -modified ceramics under 20 kV/cm; (b) The maximum cycle times; (c) Density of the 0.2 wt% Li_2CO_3 -modified ceramics; (d) Cyclically P - E curve of piezoelectric ceramics under 25 kV/cm.

4. Conclusions

In this work, the 0.2 wt% Li_2CO_3 -modified piezoelectric ceramics were developed to reduce sintering temperatures for low-temperature cofired applications. The influence of T_s on microstructure, dielectric, and piezoelectric properties was studied. Due to sintering aids, the piezoelectric ceramics could be densified at a low sintering temperature above 940 °C, suitable for co-firing with cheap electrodes. The piezoelectric ceramics can be optimized at a sintering temperature of 980 °C, accompanied by high piezoelectric $d_{33} \sim 701$ pC/N, $k_p \sim 66.7\%$, and a low $Q_m \sim 71$ with a transition temperature of $T_c \sim 226$ °C, presenting the characteristics of typical soft piezoelectric ceramics. It had a promising strain of 0.13% under a low electric field (20 kV/cm) and was competitive for the fabrication of multilayer piezoelectric transducers.

Author Contributions: Data curation, Z.L. and Z.Z.; Project administration, Z.Y. and H.H.; Supervision, Z.Y. and H.L.; Writing—original draft, Z.L., Z.Z. and H.Z.; Writing—review & editing, Z.Y., H.Z., H.H., M.C. and H.L. All authors have read and agreed to the published version of the manuscript.

Funding: This work was funded by the Natural Science Foundation of China (51872213), Sanya Science and Education Innovation Park of Wuhan University of Technology (2021KF0014), Guangdong Basic and Applied Basic Research Foundation (2021A1515110060), and Guangdong Basic and Applied Basic Research Foundation (2022A1515010073).

Data Availability Statement: The datasets generated during and analyzed during the current study are available from the corresponding author on reasonable request.

Conflicts of Interest: The authors declare no conflict of interest.

References

1. Zhang, S.J. High entropy design: A new pathway to promote the piezoelectricity and dielectric energy storage in perovskite oxides. *Microstructures* **2023**, *3*, 2023003.
2. Yao, Z.H.; Liu, H.X.; Hao, H.; Cao, M.H. Structure, electrical properties, and depoling mechanism of BiScO₃-PbTiO₃-Pb(Zn_{1/3}Nb_{2/3})O₃ high-temperature piezoelectric ceramics. *J. Appl. Phys.* **2011**, *109*, 014105. [[CrossRef](#)]
3. Gao, X.Y.; Yang, J.K.; Wu, J.G.; Xin, X.D.; Li, Z.M.; Yuan, X.T.; Shen, X.Y.; Dong, S.X. Piezoelectric actuators and motors: Materials, designs, and applications. *Adv. Mater. Technol.* **2020**, *5*, 1900716. [[CrossRef](#)]
4. Gurdal, A.E.; Tuncdemir, S.; Uchino, K.; Randall, C.A. Low temperature co-fired multilayer piezoelectric transformers for high power applications. *Mater. Des.* **2017**, *132*, 512–517. [[CrossRef](#)]
5. Wang, Q.Z.; Li, F.Z. A low-working-field (2 kV/mm), large-strain (>0.5%) piezoelectric multilayer actuator based on periodically orthogonal poled PZT ceramics. *Sens. Actuator A-Phys.* **2018**, *272*, 212–216. [[CrossRef](#)]
6. Li, Z.M.; Bian, L.; Yi, X.Y.; Zhu, R.Q.; Yuan, X.T.; Dong, S.X. A co-fired multilayer PMnS-PZT ceramic based linear piezoelectric ultrasonic micromotor with a high-load-density. *Appl. Phys. Lett.* **2022**, *120*, 082902. [[CrossRef](#)]
7. Shen, Z.Y.; Qin, C.; Luo, W.Q.; Song, F.S.; Wang, Z.M.; Li, Y.M.; Zhang, S.J. Ce and W co-doped CaBi₂Nb₂O₉ with enhanced piezoelectric constant and electrical resistivity at high temperature. *J. Mater.* **2020**, *6*, 459–466. [[CrossRef](#)]
8. Kour, P.; Pradhan, S.K.; Kumar, P.; Sinha, S.; Kar, M. Effect of Nd doping on dielectric and impedance properties of PZT nanoceramics. *J. Electron. Mater.* **2018**, *47*, 2861–2870. [[CrossRef](#)]
9. Samanta, S.; Sankaranarayanan, V.; Sethupathi, K.; Ramachandra Rao, M.S. Enhanced ferroelectricity in PLZT ceramic by precise La-doping, minimizing pyrochlore phase and lead loss. *Vacuum* **2018**, *157*, 514–523. [[CrossRef](#)]
10. Promjun, T.; Funsueb, N.; Ngamjarrojana, A. Effect of Nb, Ta and Sb addition on structure and electrical properties of PZT ceramics. *Mater. Today Proc.* **2019**, *17*, 1602–1606. [[CrossRef](#)]
11. Samanta, S.; Sankaranarayanan, V.; Sethupathi, K. Effect of successive multiple doping of La, Nb and Fe on structure and lattice vibration of MPB PZT. *Mater. Today Proc.* **2018**, *5*, 27919–27927. [[CrossRef](#)]
12. Wu, D.; Qin, S.; Liu, H.; Cao, Z.; Chen, J.F.; Fang, B.J.; Liu, C.L. Enhancing piezoelectricity of PLZT ceramics by bismuth stearate coating via water-soluble defatted powder injection molding. *Ceram. Int.* **2021**, *47*, 17956–17963. [[CrossRef](#)]
13. Kumar, A.; Raju, K.C.; Ryu, J.; James, A.R. Composition dependent Ferro-piezo hysteresis loops and energy density properties of mechanically activated (Pb_{1-x}La_x)(Zr_{0.60}Ti_{0.40})O₃ ceramics. *Appl. Phys. A-Mater. Sci. Process.* **2020**, *126*, 175. [[CrossRef](#)]
14. Chu, S.Y.; Chen, T.Y.; Tsai, I.T. Effects of sintering temperature on the dielectric and piezoelectric properties of Nb-doped PZT ceramics and their applications. *Integr. Ferroelectr.* **2003**, *58*, 1293–1303. [[CrossRef](#)]
15. Lee, W.I.; Lee, J.K. Dopant effects on the grain structure and electrical property of PZT thin films prepared by sol-gel process. *Mater. Res. Bull.* **1995**, *30*, 1185–1191. [[CrossRef](#)]
16. Yan, S.; Sun, C.; Cui, Q.Y.; He, M.Z.; Willhandy; Wang, R.B.; Hao, J.J.; Chu, X.C. Dielectric, piezoelectric and dc bias characteristics of Bi-doped PZT multilayer ceramic actuator. *Mater. Chem. Phys.* **2020**, *255*, 123605. [[CrossRef](#)]
17. Zeng, Z.Q.; Wu, Q.C.; Hao, M.M.; Lu, W.Z.; Fan, G.F.; Ming, Y.C.; Ding, M.Y. Impedance spectroscopy and piezoelectric property of LiF-doped PZN-PZT low-temperature sintering piezoelectric ceramics. *J. Mater. Sci.-Mater. Electron.* **2018**, *29*, 8279–8286. [[CrossRef](#)]
18. Zhang, M.H.; Wang, K.; Du, Y.J.; Dai, G.; Sun, W.; Li, G.; Hu, D.; Thong, H.C.; Zhao, C.L.; Xi, X.Q. High and temperature-insensitive piezoelectric strain in Alkali niobate lead-free perovskite. *J. Am. Chem. Soc.* **2017**, *139*, 3889–3895. [[CrossRef](#)]
19. Ghasemifard, M.; Hosseini, S.M.; Zak, A.K.; Khorrami, G.H. Microstructural and optical characterization of PZT nano-powder prepared at low temperature. *Phys. E Low-Dimens. Syst. Nanostruct.* **2009**, *41*, 418–422. [[CrossRef](#)]
20. Corker, D.L.; Whatmore, R.W.; Ringgaard, E.; Wolny, W.W. Liquid-phase sintering of PZT ceramics. *J. Eur. Ceram. Soc.* **2000**, *20*, 2039–2045. [[CrossRef](#)]
21. Guo, J.; Guo, H.; Baker, A.L.; Lanagan, M.T.; Kupp, E.R.; Messing, G.L.; Randall, C.A. Cold sintering: A paradigm shift for processing and integration of ceramics. *Angew. Chem. Int. Ed.* **2016**, *55*, 11457–11461. [[CrossRef](#)] [[PubMed](#)]
22. Siddiqui, M.; Mohamed, J.J.; Ahmad, Z.A. Structural properties of Pb(Zr_{0.52}Ti_{0.38}Li_{0.1})O₃ prepared via high planetary mill. *Mater. Sci. Forum.* **2017**, *888*, 91–95.
23. Jan, H.; Francesco, P.; Sona, H.; Vojtech, N. Sintering aids, their role, and behavior in the production of transparent ceramics. *Open Ceram.* **2021**, *7*, 100137.
24. Zhang, W.L.; Eitel, R.E. Low-temperature sintering and properties of 0.98PZT-0.02SKN ceramics with LiBiO₂ and CuO addition. *J. Am. Ceram. Soc.* **2011**, *94*, 3386–3390. [[CrossRef](#)]
25. Choi, J.J.; Hahn, B.D.; Park, D.S.; Yoon, W.H.; Lee, J.H.; Jang, J.H.; Ko, K.H.; Park, C. Low-temperature sintering of lead zinc niobate-lead zirconate titanate ceramics using nano-sized powder prepared by the stirred media milling process. *J. Am. Ceram. Soc.* **2007**, *90*, 388–392. [[CrossRef](#)]
26. Donnelly, N.J.; Shrout, T.R.; Randall, C.A. The role of Li₂CO₃ and PbO in the low-temperature sintering of Sr, K, Nb (SKN)-doped PZT. *J. Am. Ceram. Soc.* **2009**, *92*, 1203–1207. [[CrossRef](#)]
27. Siddiqui, M.; Mohamed, J.J.; Ahmad, Z.A. Piezoelectric and dielectric properties of Pb_{0.93}La_{0.02}Sr_{0.05}(Zr_{0.52}Ti_{0.48})O₃ ceramics doped with Li₂CO₃ at low sintering temperature. *Ceram. Int.* **2016**, *43*, 2644–2649. [[CrossRef](#)]

28. Kim, B.S.; Ji, J.H.; Koh, J.H. Improved strain and transduction values of low-temperature sintered CuO-doped PZT-PZNN soft piezoelectric materials for energy harvester applications. *Ceram. Int.* **2021**, *47*, 6683–6690. [[CrossRef](#)]
29. Zhang, S.K.; Guo, F.F.; Jia, B.; Zhou, H.Q.; Dai, Z.H.; Xi, Z.Z. Effect of Li_2CO_3 on the structure and electrical properties of low-temperature-sintered 15PSN-52PMN-33PT ceramics. *J. Am. Ceram. Soc.* **2022**, *33*, 2044–2051. [[CrossRef](#)]
30. Quang, D.A.; Vuong, L.D. Enhanced piezoelectric properties of Fe_2O_3 and Li_2CO_3 co-doped $\text{Pb}[(\text{Zr}_{0.48}\text{Ti}_{0.52})_{0.8}(\text{Zn}_{1/3}\text{Nb}_{2/3})_{0.125}(\text{Mn}_{1/3}\text{Nb}_{2/3})_{0.075}]\text{O}_3$ ceramics for ultrasound transducer application. *J. Mater. Sci. Adv. Mater. Dev.* **2022**, *7*, 100436.
31. Gao, X.Y.; Jin, H.N.; Xin, B.J.; Wang, M.W.; Dong, S.X.; Xu, Z.; Li, F. Low-temperature sintering of Li_2CO_3 added $\text{Pb}(\text{Ni}_{1/3}\text{Nb}_{2/3})$ - $\text{Pb}(\text{Zr,Ti})\text{O}_3$ ceramics with high piezoelectric properties. *J. Alloys Compd.* **2022**, *892*, 162132. [[CrossRef](#)]
32. Fan, G.F.; Shi, M.B.; Lu, W.Z.; Wang, Y.Q.; Liang, F. Effects of Li_2CO_3 and Sm_2O_3 additives on low-temperature sintering and piezoelectric properties of PZN-PZT ceramics. *J. Eur. Ceram. Soc.* **2014**, *34*, 23–28. [[CrossRef](#)]
33. Zhang, Q.; Yue, Y.; Nie, R.; Liu, H.; Chen, Q.; Yu, P.; Zhu, J.G.; Xiao, D.Q. Achieving both high d_{33} and high TC in low-temperature sintering $\text{Pb}(\text{Ni}_{1/3}\text{Nb}_{2/3})\text{O}_3$ - $\text{Pb}(\text{Mg}_{1/2}\text{W}_{1/2})\text{O}_3$ - $\text{Pb}(\text{Zr}_{0.5}\text{Ti}_{0.5})\text{O}_3$ ceramics using Li_2CO_3 . *Mater. Res. Bull.* **2017**, *85*, 96–103. [[CrossRef](#)]
34. Chen, H.; Xing, J.; Xi, J.W.; Pu, T.; Liu, H.; Zhu, J.G. Origin of high piezoelectricity in low-temperature sintering PZT-based relaxor ferroelectric ceramics. *J. Alloys Compd.* **2020**, *860*, 157930. [[CrossRef](#)]
35. Chen, H.; Pu, T.; Fan, S.B.; Liu, H.; Zhu, J.G.; Chen, Q. Enhanced electrical properties in low-temperature sintering PNN-PMW-PZT ceramics by Yb_2O_3 doping. *Mater. Res. Bull.* **2022**, *146*, 111576. [[CrossRef](#)]
36. Nie, R.; Zhang, Q.; Yue, Y.; Liu, H.; Chen, Q.; Zhu, J.G.; Yu, P.; Xiao, D.Q. Properties of Low-Temperature Sintering PNN-PMW-PSN-PZT Piezoelectric Ceramics with $\text{Ba}(\text{Cu}_{1/2}\text{W}_{1/2})\text{O}_3$ Sintering Aids. *Int. J. Appl. Ceram. Technol.* **2016**, *13*, 1119–1124. [[CrossRef](#)]
37. Yang, S.L.; Tsai, C.C.; Hong, C.S.; Chu, S.Y. Effects of sintering aid CuTa_2O_6 on piezoelectric and dielectric properties of sodium potassium niobate ceramics. *Mater. Res. Bull.* **2012**, *47*, 998–1003. [[CrossRef](#)]
38. Chen, Y.; Xie, S.X.; Wang, Q.Y.; Fu, L.; Nie, R.; Zhu, J.G. Correlation between microstructural evolutions and electrical/mechanical behaviors in Nb/Ce co-doped $\text{Pb}(\text{Zr}_{0.52}\text{Ti}_{0.48})\text{O}_3$ ceramics at different sintering temperatures. *Mater. Res. Bull.* **2017**, *94*, 174–182. [[CrossRef](#)]
39. Dong, Y.Z.; Zhou, Z.Y.; Liang, R.H.; Dong, X.L. Correlation between the grain size and phase structure, electrical properties in BiScO_3 - PbTiO_3 -based piezoelectric ceramics. *J. Am. Ceram. Soc.* **2020**, *103*, 4785–4793. [[CrossRef](#)]
40. Zheng, M.P.; Hou, Y.D.; Ge, H.Y.; Zhu, M.K.; Yan, H. Effect of NiO additive on microstructure, mechanical behavior and electrical properties of 0.2PZN-0.8PZT ceramics. *J. Eur. Ceram. Soc.* **2013**, *33*, 1447–1456. [[CrossRef](#)]
41. Du, Z.Z.; Zhao, C.L.; Thong, H.C.; Zhou, Z.; Zhou, J.J.; Wang, K.; Guan, C.L.; Liu, H.; Fang, J.Z. Effect of MnCO_3 on the electrical properties of PZT-based piezoceramics sintered at low temperature. *J. Alloys Compd.* **2019**, *801*, 27–32. [[CrossRef](#)]
42. Geng, W.P.; Chen, X.; Pan, L.; Qiao, X.J.; He, J.; Mu, J.L.; Hou, X.J.; Chou, X.J. Improved crystallization, domain, and ferroelectricity by controlling lead/oxygen vacancies in Mn-doped PZT thin films. *Mater. Charact.* **2021**, *176*, 111131. [[CrossRef](#)]
43. Beom, H.G.; Jeong, K.M.; Park, J.Y.; Lin, S.; Kim, G.H. Electrical failure of piezoelectric ceramics with a conductive crack under electric fields. *Eng. Fract. Mech.* **2009**, *76*, 2399–2407. [[CrossRef](#)]

Disclaimer/Publisher's Note: The statements, opinions and data contained in all publications are solely those of the individual author(s) and contributor(s) and not of MDPI and/or the editor(s). MDPI and/or the editor(s) disclaim responsibility for any injury to people or property resulting from any ideas, methods, instructions or products referred to in the content.